Nigerian Journal of Physics (NJP)
ISSN online: 3027-0936
ISSN print: 1595-0611
DOI: https://doi.org/10.62292/njp.v35i1.2026.476
Volume 35(1), March 2026

Energy Values of Titanium Hydride (TiH) Diatomic Molecule with Modified Kratzer Energy-Dependent Screened Coulomb Potential in the Presence of Magnetic and Aharonov-Bohm Flux Fields

[1]Ishaya Sunday Danladi, [2]Yakubu Yerima Jabil and [2]Lawrence Davou Christopher

[1]NNPC Downstream Investment Service, NNPC Towers, FCT Abuja, Nigeria.
[2]Department of Physics, University of Jos, Plateau State, Nigeria.

*Corresponding Author's Email: ishayadan@gmail.com

ABSTRACT

In this study, the modified Kratzer energy-dependent screened Coulomb potential is analyzed in the presence of external magnetic and Aharonov–Bohm (AB) flux fields. The Schrödinger equation is solved using the Nikiforov–Uvarov Functional Analysis (NUFA) method, yielding closed-form expressions for the energy eigenvalues and the corresponding wavefunctions. The resulting solutions are applied to the Titanium Hydride (TiH) diatomic molecule to investigate how external fields and the slope parameter $\tilde{g}$ which characterizes the rate at which the screening strength and potential shape vary with internuclear separation affect the molecular energy spectrum. The slope parameter plays a key role in determining the stiffness and depth of the effective potential: negative values ($\tilde{g} < 0$) enhance attractive behavior and support both positive and negative bound-state energies; zero slope ($\tilde{g} = 0$) produces only positive bound-state levels; and positive slope ($\tilde{g} > 0$) alters the spacing of the spectrum by increasing the sensitivity of the energy levels to external-field perturbations. Numerical results show that external fields strongly influence degeneracy patterns in TiH. Magnetic fields remove degeneracy across $m = \pm 1$, AB-flux fields create quasi-degeneracy, and the combined fields produce the most significant degeneracy lifting. Energy values consistently decrease with increasing vibrational quantum number n. Special cases obtained by varying the magnetic quantum number and slope parameter reduce to the known modified Kratzer–Coulomb potential, and the resulting spectra agree well with available literature. These findings highlight the sensitivity of TiH molecular states to the slope parameter and external fields.

Keywords:
Aharonov–Bohm (AB) flux,
Energy-dependent screened Coulomb potential,
Modified Kratzer potential,
Slope parameter,
Titanium Hydride (TiH) diatomic molecule

INTRODUCTION

In quantum mechanics, solving the Schroedinger equation is critical for understanding the energy spectrum and other properties of quantum systems (Flugge, 1971). The solutions to this equation provide energy eigenvalues and eigenfunctions, which are essential for understanding the quantum states of particles or systems. These solutions are used in a range of applications, from determining energy levels in atoms and molecules to investigating mass spectra in quarkonia systems (Ibekwe *et al*., 2021), thermodynamic properties of quantum systems (Jia, Zhang & Wang, 2017), and even quantum information theory (Ikot *et al*., 2020). A wealth of research has been devoted to obtaining analytical solutions of the SE for various potential models. Among the most studied potentials are the Deng–Fan potential (Edet *et al*., 2022), the Improved Ultra-Generalized Exponential Hyperbolic Potential (Ikot *et al*., 2021), the Inverse Quadratic Yukawa potential (Horchani *et al*., 2021), and the Modified Kratzer potential (Onyenegecha *et al*., 2021), to name just a few. The energy eigenvalues and wavefunctions associated with these potentials are of paramount importance for understanding the physical properties of quantum systems, such as their bound states, transitions, and spectrum.

To solve the SE for these potentials, various mathematical techniques have been employed. These include the Nikiforov-Uvarov (NU) method (Nikiforov & Uvarov, 1988), the Nikiforov-Uvarov-Functional Analysis (NUFA) method (Ikot *et al*., 2021), the Extended Nikiforov-Uvarov (ENU) method (Karayer, Demirha & Buyukkilic, 2015), and the parametric NU

method (Tezcan & Sever, 2009), among others. Other techniques, such as the formula method (Falaye, Ikhdair & Hamzavi, 2015) and the Proper Quantization Rule (PQR) method (Serrano, Gu & Dong, 2010), have also been used to extract the energy eigenvalues and eigenfunctions. These methods are essential for solving the SE in situations where analytical solutions are difficult to obtain, particularly in systems with complex potential profiles.

In recent years, a considerable body of work has emerged in the literature focusing on the effects of magnetic fields and Aharonov-Bohm (AB) flux fields on various quantum systems. These studies employ a wide range of analytical techniques and potential models to explore their impact. For example, using the asymptotic iteration method, (Aygun, Bayrak, Boztosun & Sahin, 2012) derived the energy eigenvalues of the Kratzer potential, both with and without the influence of a constant magnetic field, within the context of the 2D Schrödinger wave equation. Eshghi & Mehraban (2017) examined the behavior of a particle confined by both magnetic and AB flux fields under a radial scalar power potential. Additionally, Ikhdair, Hamzavi & Sever (2012) as well as Ikhdair & Hamzavi (2012) studied 2D harmonic and pseudo-harmonic oscillators in the presence of external fields, calculating the energy spectrum and wave functions for electrons in these systems. Similarly, Khordad (2010) & Cetin (2008) explored eigensolutions for a charged particle confined by a harmonic oscillator in the presence of both a strong magnetic field and an AB flux field, investigating various spectral properties. Ferkous & Bounames (2013) solved the 2D Pauli equation with the Hulthen potential for a spin-1/2 particle under the influence of an AB flux field, while Ferkous, Boultif & Sifour (2019) derived bound-state energy eigenvalues for a spin-1/2 particle subjected to the modified Pöschl-Teller potential in the presence of an AB field, further exploring the interaction between spin and magnetic flux. Nevertheless, despite the breadth of existing studies, our review indicates that the modified Kratzer energy-dependent screened Coulomb potential has not yet been investigated in the presence of external magnetic and Aharonov–Bohm (AB) flux fields to study the energy values of the titanium hydride. Addressing this gap constitutes the central objective of the present work. The modified Kratzer energy-dependent screened Coulomb potential is expressed as:

$$V(r,E_{nm}) = D_e\left(\frac{r-r_e}{r}\right)^2 - \frac{C}{r}(1+\tilde{g}E_{nm})e^{-\delta r} \quad (1)$$

where D_e is the dissociation energy, r_e is the equilibrium internuclear separation, C is the depth of the potential, δ is the screening parameter, and $\tilde{g}$ is the slope parameter and can be adjusted as desired.

MATERIALS AND METHODS

In this section, we briefly introduce the Nikiforov-Uvarov Functional Analysis (NUFA) method (Ikot *et. al.,* 2021). This method is useful in solving second-order differential wave equations of the hypergeometric-type (Ikot *et. al.,* 2021):

$$\frac{d^2\psi(s)}{ds^2} + \frac{\tilde{\tau}(s)}{\sigma(s)}\frac{d\psi(s)}{ds} + \frac{\tilde{\sigma}(s)}{\sigma^2(s)}\psi(s) = 0 \quad (2)$$

where $\sigma(s)$ and $\tilde{\sigma}(s)$ are polynomials of at most second degree, and $\tilde{\tau}(s)$, is a first degree polynomial. Tezcan & Sever (2008), latter introduced the parametric form of NU method in the form

$$\frac{d^2\psi(s)}{ds^2} + \frac{\alpha_1-\alpha_2 s}{s(1-\alpha_3 s)}\frac{d\psi(s)}{ds} + \frac{1}{s^2(1-\alpha_3 s)^2}[-\xi_1 s^2 + \xi_2 s - \xi_3]\psi(s) = 0 \quad (3)$$

where α_i and $\xi_i (i = 1,2,3)$ are all parameters. It can be observed in Eq. (3) that the differential equation has two singularities at $s \to 0$ and $s \to 1$, thus it takes the wave function in the form

$$\psi(s) = s^{\lambda}(1-s)^{v} f(s) \quad (4)$$

Substituting Eq. (4) into Eq. (3) leads to the following equation

$$s(1-\alpha_3 s)\frac{d^2f(s)}{ds^2} + [\sigma_1 + 2\lambda - (2\lambda\alpha_3 + 2v\alpha_3 + \alpha_2)s]\frac{df(s)}{ds} - \alpha_3\left(\lambda + v + \frac{1}{2}\left(\frac{\alpha_2}{\alpha_3} - 1\right) + \sqrt{\frac{1}{4}\left(\frac{\alpha_2}{\alpha_3} - 1\right)^2 + \frac{\xi_1}{\alpha_3^2}}\right)\left(\lambda + v + \frac{1}{2}\left(\frac{\alpha_2}{\alpha_3} - 1\right) - \sqrt{\frac{1}{4}\left(\frac{\alpha_2}{\alpha_3} - 1\right)^2 + \frac{\xi_1}{\alpha_3^2}}\right) + \left[\frac{\lambda(\lambda-1)+\alpha_1\lambda-\xi_3}{s} + \frac{v(v-1)\alpha_3+\alpha_2 v-\alpha_1\alpha_3 v-\frac{\xi_1}{\alpha_3}+\xi_2-\xi_3\alpha_3}{(1-\alpha_3 s)}\right]f(s) = 0 \quad (5)$$

Eq. (5) can be reduced to a Gauss hypergeometric equation if and only if the following functions vanish

$$\lambda(\lambda-1) + \alpha_1\lambda - \xi_3 = 0 \quad (6)$$

$$v(v-1)\alpha_3 + \alpha_2 v - \alpha_1\alpha_3 v - \frac{\xi_1}{\alpha_3} + \xi_2 - \xi_3\alpha_3 = 0 \quad (7)$$

Thus, Eq. (5) now becomes

$$s(1-\alpha_3 s)\frac{d^2f(s)}{ds^2} + [\sigma_1 + 2\lambda - (2\lambda\alpha_3 + 2v\alpha_3 + \alpha_2)s]\frac{df(s)}{ds} - \alpha_3\left(\lambda + v + \frac{1}{2}\left(\frac{\alpha_2}{\alpha_3} - 1\right) + \sqrt{\frac{1}{4}\left(\frac{\alpha_2}{\alpha_3} - 1\right)^2 + \frac{\xi_1}{\alpha_3^2}}\right)\times\left(\lambda + v + \frac{1}{2}\left(\frac{\alpha_2}{\alpha_3} - 1\right) - \sqrt{\frac{1}{4}\left(\frac{\alpha_2}{\alpha_3} - 1\right)^2 + \frac{\xi_1}{\alpha_3^2}}\right)f(s) = 0 \quad (8)$$

Solving Eqs. (6) and (7) completely give

$$\lambda = \frac{1}{2}\left((1-\alpha_1) \pm \sqrt{(1-\alpha_1)^2 + 4\xi_3}\right) \tag{9}$$

$$v = \frac{1}{2\alpha_3}\left((\alpha_3 + \alpha_1\alpha_3 - \alpha_2) \pm \sqrt{(\alpha_3 + \alpha_1\alpha_3 - \alpha_2)^2 + 4\left(\frac{\xi_1}{\alpha_3} + \alpha_3\xi_3 - \xi_2\right)}\right) \tag{10}$$

Eq. (8) is the hypergeometric equation type of the form

$$x(1-x)\frac{d^2f(x)}{dx^2} + [c + (a+b+1)x]\frac{df(x)}{dx} - [ab]f(x) = 0 \tag{11}$$

where a, b, and c are given as follows

$$a = \sqrt{\alpha_3}\left(\lambda + v + \frac{1}{2}\left(\frac{\alpha_2}{\alpha_3} - 1\right) + \sqrt{\frac{1}{4}\left(\frac{\alpha_2}{\alpha_3} - 1\right)^2 + \frac{\xi_1}{\alpha_3^2}}\right) \tag{12}$$

$$b = \sqrt{\alpha_3}\left(\lambda + v + \frac{1}{2}\left(\frac{\alpha_2}{\alpha_3} - 1\right) - \sqrt{\frac{1}{4}\left(\frac{\alpha_2}{\alpha_3} - 1\right)^2 + \frac{\xi_1}{\alpha_3^2}}\right) \tag{13}$$

$$c = \alpha_1 + 2\lambda \tag{14}$$

Setting either $a$or b equal to a negative integer$-n$, the hypergeometric function $f(s)$ turns to a polynomial of degree n. Hence, the hypergeometric function $f(s)$ approaches finite in the following quantum condition i.e. $a = -n$, where $n = 0,1,2,3,\ldots.n_{max}$

Using the above quantum condition,

$$\sqrt{\alpha_3}\left(\lambda + v + \frac{1}{2}\left(\frac{\alpha_2}{\alpha_3} - 1\right) + \sqrt{\frac{1}{4}\left(\frac{\alpha_2}{\alpha_3} - 1\right)^2 + \frac{\xi_1}{\alpha_3^2}}\right) = -n \tag{15}$$

$$\lambda + v + \frac{1}{2}\left(\frac{\alpha_2}{\alpha_3} - 1\right) + \frac{n}{\sqrt{\alpha_3}} = -\sqrt{\frac{1}{4}\left(\frac{\alpha_2}{\alpha_3} - 1\right)^2 + \frac{\xi_1}{\alpha_3^2}} \tag{16}$$

Squaring both sides of Eq. (16) and rearranging, one obtains the energy equation for the NUFA method as

$$\lambda^2 + 2\lambda\left(v + \frac{1}{2}\left(\frac{\alpha_2}{\alpha_3} - 1\right) + \frac{n}{\sqrt{\alpha_3}}\right) + \left(v + \frac{1}{2}\left(\frac{\alpha_2}{\alpha_3} - 1\right) + \frac{n}{\sqrt{\alpha_3}}\right)^2 - \frac{1}{4}\left(\frac{\alpha_2}{\alpha_3} - 1\right)^2 - \frac{\xi_1}{\alpha_3^2} = 0 \tag{17}$$

By substituting Eqs. (9) and (10) into Eq. (4), one obtains the corresponding wave equation for the NUFA method as:

$$\psi(s) = \mathbb{N}s^{\frac{(1-\alpha_1)+\sqrt{(\alpha_1-1)^2+4\xi_3}}{2}}(1-\alpha_3 s)^{\frac{(\alpha_3+\alpha_1\alpha_3-\alpha_2)+\sqrt{(\alpha_3+\alpha_1\alpha_3-\alpha_2)^2+4\left(\frac{\xi_1}{\alpha_3}+\alpha_3\xi_3-\xi_2\right)}}{2\alpha_3}}{}_2F_1(a,b,c;s) \tag{18}$$

where $\mathbb{N}$ is the normalization constant.

Only the positive sign is used above because it ensures a normalizable, physically acceptable wavefunction and produces discrete bound-state energies, while the negative sign leads to divergent or non-physical solutions.

Solution of the 2D Schrodinger Equation TiH Diatomic Molecule with Magnetic and AB-flux Fields

A generalized form of the Schrodinger Equation (SE) for a charged particle moving under the influence of the vector potential $\vec{A}$ is written as (Purohit *et al*., 2020; Rampho *et al*., 2020; Ikot *et al*., 2020):

$$\left(i\hbar\vec{\nabla} + \frac{e}{c}\vec{A}\right)^2\psi(r,\phi) = 2\mu[E_{nm} - V(r)]\psi(r,\phi) \tag{19}$$

where e and μ are the charge of the particle and reduced mass of the system respectively, E_{nm} is the energy eigenvalues, $c$is the velocity of light, $\vec{A}$ is the vector potential and $V(r)$ scalar potential. To indicate the magnetic field and AB-flux field together, we express the vector potential $\vec{A}$ as a sum of two terms $\vec{A} = \vec{A}_1 + \vec{A}_2$having azimuthal components as (Purohit et al., 2020; Rampho et al., 2020; Ikot et al., 2020; 2021):

$$\vec{A}_1 = \frac{\vec{B}e^{-\delta r}}{1-e^{-\delta r}}\hat{\phi} \text{ and } \vec{A}_2 = \frac{\Phi_{AB}}{2\pi r}\hat{\phi} \tag{20}$$

where $\vec{B}$ is the applied external magnetic field with $\vec{\nabla}\times\vec{A}_1 = \vec{B}, \vec{A}_2$represents the additional magnetic flux $\Phi_{\mathrm{AB}} = \xi$ created by a solenoid with $\vec{\nabla}\cdot\vec{A}_2 = 0$. Then the vector potential $\vec{A}$ can be written as:

$$\vec{A} = \left(\frac{\vec{B}e^{-\delta r}}{1-e^{-\delta r}} + \frac{\xi}{2\pi r}\right)\hat{\phi} \tag{21}$$

where $\hat{\phi}$ is the direction of magnetic flux around the solenoid. Also, we assume a wavefunction in the cylindrical coordinates to be of the form:

$$\psi(r,\phi) = (2\pi r)^{-\frac{1}{2}}e^{im\phi}\Omega_{nm}(r) \tag{22}$$

where m is the magnetic quantum number.

Substituting Eq. (1) into Eq. (19), we have

$$\left(i\hbar\vec{\nabla}+\frac{e}{c}\vec{A}\right)^2\psi(r,\phi)=2\mu\left[E_{nm}-D_e\left(\frac{r-r_e}{r}\right)^2+\frac{C}{r}(1+\tilde{g}E_{nm})e^{-\delta r}\right]\psi(r,\phi) \tag{23}$$

For convenience, let us introduce $\lambda=\frac{e}{c}$, so that Eq. (23) becomes

$$\left(i\hbar\vec{\nabla}+\lambda\vec{A}\right)^2\psi(r,\phi)=2\mu\left[E_{nm}-D_e+\frac{2D_er_e}{r}-\frac{D_er_e^2}{r^2}+\frac{C}{r}e^{-\delta r}+\frac{C\tilde{g}E_{nm}}{r}e^{-\delta r}\right]\psi(r,\phi) \tag{24}$$

Using Eqs. (21) and (22) into Eq. (24) we get the 2nd order differential equation (DE) given as follows:

$$\Omega''_{nm}(r)+\left[\begin{matrix}\frac{2\mu}{\hbar^2}\left(E_{nm}-D_e+\frac{2D_er_e}{r}-\frac{D_er_e^2}{r^2}+\frac{C}{r}e^{-\delta r}+\frac{C\tilde{g}E_{nm}}{r}e^{-\delta r}\right)+\frac{1}{4r^2}-\frac{m^2}{r^2}\\+\frac{2m\lambda\vec{B}e^{-\delta r}}{\hbar(1-e^{-\delta r})r}+\frac{m\lambda\xi}{\hbar\pi r^2}-\frac{\lambda^2\vec{B}^2e^{-2\delta r}}{\hbar^2(1-e^{-\delta r})^2}-\frac{\lambda^2\vec{B}\xi e^{-\delta r}}{\hbar^2(1-e^{-\delta r})\pi r}-\frac{\lambda^2\xi^2}{4\pi^2\hbar^2r^2}\end{matrix}\right]\Omega_{nm}(r)=0 \tag{25}$$

Equation (25) is a complicated differential equation that cannot be solved easily due to the presence of centrifugal $\frac{1}{r^2}$ as well as the reciprocal $\frac{1}{r}$ terms. Therefore, to bypass these terms we introduce the Greene-Aldrich approximation scheme (Greene & Aldrich, 1976). These approximations are given by:

$$\frac{1}{r^2}\approx\frac{\delta^2}{(1-e^{-\delta r})^2}\text{ and}\frac{1}{r}\approx\frac{\delta}{(1-e^{-\delta r})} \tag{26}$$

Using the approximation terms of Eqs. (26) into Eq. (25) we have:

$$\Omega''_{nm}(r)+\left[\begin{matrix}\frac{2\mu E_{nm}}{\hbar^2}-\frac{2\mu D_e}{\hbar^2}+\frac{4\mu\delta D_er_e}{\hbar^2(1-e^{-\delta r})}-\frac{2\mu\delta^2D_er_e^2}{\hbar^2(1-e^{-\delta r})^2}\\+\frac{2\mu\delta C}{\hbar^2(1-e^{-\delta r})}e^{-\delta r}+\frac{2\mu\delta C\tilde{g}E_{nm}}{\hbar^2(1-e^{-\delta r})}e^{-\delta r}+\frac{2m\delta\lambda\vec{B}}{\hbar(1-e^{-\delta r})^2}e^{-\delta r}\\-\frac{\lambda^2\vec{B}^2}{\hbar^2(1-e^{-\delta r})^2}e^{-2\delta r}-\frac{\lambda^2\delta\vec{B}\xi}{\hbar^2\pi(1-e^{-\delta r})^2}e^{-\delta r}\\-\frac{\left[(m-\gamma)^2-\frac{1}{4}\right]\delta^2}{(1-e^{-\delta r})^2}\end{matrix}\right]\Omega_{nm}(r)=0 \tag{27}$$

where we have defined the following parameters as $\phi_0=\frac{hc}{e}$ and $\gamma=\frac{\xi}{\phi_0}$.

Now introducing the NUFA method of Eq. (3) into Eq. (27) with the following coordinate transformation $z=e^{-\delta r}$. Equation (27) becomes

$$\frac{d^2\Omega_{nm}(r)}{dz^2}+\frac{1}{z}\frac{d\Omega_{nm}(r)}{dz}+\frac{1}{z^2}\left[\begin{matrix}\frac{2\mu E_{nm}}{\hbar^2\delta^2}-\frac{2\mu D_e}{\hbar^2\delta^2}+\frac{4\mu D_er_e}{\hbar^2\delta(1-z)}-\frac{2\mu D_er_e^2}{\hbar^2(1-z)^2}\\+\frac{2\mu C}{\hbar^2\delta(1-z)}z+\frac{2\mu C\tilde{g}E_{nm}}{\hbar^2\delta(1-z)}z+\frac{2m\lambda\vec{B}}{\hbar\delta(1-z)^2}z\\-\frac{\lambda^2\vec{B}^2}{\hbar^2\delta^2(1-z)^2}z^2-\frac{\lambda^2\vec{B}\xi}{\hbar^2\pi\delta(1-z)^2}z-\frac{\left[(m-\gamma)^2-\frac{1}{4}\right]}{(1-z)^2}\end{matrix}\right]\Omega_{nm}(r)=0 \tag{28}$$

To make Eq. (28) solvable with NUFA method, let's introduce the following dimensionless parameters

$$-\varepsilon_{nm}=\frac{2\mu E_{nm}}{\hbar^2\delta^2},Q_1=-\frac{2\mu D_e}{\hbar^2\delta^2},Q_2=\frac{4\mu D_er_e}{\hbar^2\delta},Q_3=-\frac{2\mu D_er_e^2}{\hbar^2},Q_4=\frac{2\mu C}{\hbar^2\delta},Q_5=\frac{2\mu a\tilde{g}E_{nm}}{\hbar^2\delta},Q_6=\frac{2m\lambda\vec{B}}{\hbar\delta},Q_7=-\frac{\lambda^2\vec{B}^2}{\hbar^2\delta^2},$$
$$Q_8=-\frac{\lambda^2\vec{B}\xi}{\hbar^2\delta\pi},Q_9=-\left[(m-\gamma)^2-\frac{1}{4}\right] \tag{29}$$

$$\frac{d^2\Omega_{nm}(r)}{dz^2}+\frac{1}{z}\frac{d\Omega_{nm}(r)}{dz}+\frac{1}{z^2}\left[\begin{matrix}-\varepsilon_{nm}+Q_1+\frac{Q_2}{(1-z)}+\frac{Q_3}{(1-z)^2}+\frac{Q_4z}{(1-z)}+\frac{Q_5z}{(1-z)}\\+\frac{Q_6z}{(1-z)^2}+\frac{Q_7z^2}{(1-z)^2}+\frac{Q_8z}{(1-z)^2}+\frac{Q_9}{(1-z)^2}\end{matrix}\right]\Omega_{nm}(r)=0 \tag{30}$$

and for mathematical simplicity and convenience Eq. (30) becomes:

$$\frac{d^2\Omega_{nm}(r)}{dz^2}+\frac{(1-z)}{z(1-z)}\frac{d\Omega_{nm}(r)}{dz}+\frac{1}{z^2(1-z)^2}[-(\varepsilon_{nm}+p_1)z^2+(2\varepsilon_{nm}+p_2)z-(\varepsilon_{nm}+p_3)]\Omega_{nm}(r)=0 \tag{31}$$

Where

$$p_1=-Q_1+Q_4+Q_5-Q_7,\quad p_2=-2Q_1-Q_2+Q_4+Q_5+Q_6+Q_8,p_3=-Q_1-Q_2-Q_3-Q_9 \tag{32}$$

And

$$\alpha_1=\alpha_2=\alpha_3=1,\ \xi_1=\varepsilon_{nm}+p_1,\ \xi_2=2\varepsilon_{nm}+p_2,\ \xi_3=\varepsilon_{nm}+p_3 \tag{33}$$

By comparing Eq. (31) with the NUFA method of Eq. (3), then we obtain the following (Ikot *et al*., 2021):

$$\lambda=\sqrt{\varepsilon_{nm}+p_3} \tag{34}$$

And

$$v=\frac{1}{2}+\sqrt{\frac{1}{4}+\xi_1-\xi_2+\xi_3} \tag{35}$$

Substituting Eqs. (33), (34) and (35) into Eq. (17), we get the energy eigenvalues as:

$$\varepsilon_{nm} + p_3 = \left[\frac{p_1 - p_3 - (n+v)^2}{2(n+v)}\right]^2 \tag{36}$$

Substituting Eqs. (29) and (32) into Eq. (36), we get

$$E_{nm} = D_e - 2D_e\delta r_e + D_e\delta^2 r_e^2 + \frac{\hbar^2\delta^2}{2\mu}\left[(m-\gamma)^2 - \frac{1}{4}\right] - \frac{\hbar^2\delta^2}{2\mu}\left[\frac{\frac{2\mu C}{\hbar^2\delta} + \frac{2\mu C\tilde{g}E_{nm}}{\hbar^2\delta} + \frac{\tilde{\lambda}^2\vec{B}^2}{\hbar^2\delta^2} + \frac{4\mu D_e r_e}{\hbar^2\delta} - \frac{2\mu D_e r_e^2}{\hbar^2} - \left[(m-\gamma)^2 - \frac{1}{4}\right] - (n+v)^2}{2(n+v)}\right]^2 \tag{37}$$

Where

$$\lambda = \frac{1}{2} + \sqrt{\frac{\tilde{\lambda}^2\vec{B}^2}{\hbar^2\delta^2} + \frac{2\mu D_e r_e^2}{\hbar^2} + (m-\gamma)^2 - \frac{2m\tilde{\lambda}\vec{B}}{\hbar\delta} + \frac{\tilde{\lambda}^2\vec{B}\xi}{\hbar^2\delta\pi}} \tag{38}$$

Equation (37) is an implicit self-consistent equation for the bound-state energy E_{nm}, as it appears on both sides. It is solved numerically using an iterative procedure, starting from an initial guess and updating until convergence is achieved within a specified tolerance. Some optional methods of solution includes fixed-point iteration, Newton–Raphson, or solve.

Substituting Eqs. (29), (32) and (33) into Eq. (18), the corresponding Energy eigenfunction equation can be obtained as:

$$\Omega_{nm}(z) = \aleph_{n\ell} z^{\sqrt{-\frac{2\mu E_{nm}}{\hbar^2\delta^2} + \frac{2\mu D_e}{\hbar^2\delta^2} - \frac{4\mu D_e r_e}{\hbar^2\delta} + \frac{2\mu D_e r_e^2}{\hbar^2} + \left[(m-\gamma)^2 - \frac{1}{4}\right]}} \times (1-z)^{\frac{1}{2} + \sqrt{\frac{1}{4} + \frac{2\mu D_e}{\hbar^2\delta^2} + \frac{2\mu C}{\hbar^2\delta} + \frac{2\mu C\tilde{g}E_{nm}}{\hbar^2\delta} + \frac{\lambda^2\vec{B}^2}{\hbar^2\delta^2}}} {}_2F_1(a,b,c;z) \tag{39}$$

Where

$$a = \beta + \sigma + \sqrt{\varepsilon_{nm} + p_1} \tag{40}$$

$$b = \beta + \sigma - \sqrt{\varepsilon_{nm} + p_1} \tag{41}$$

$$c = 1 + 2\beta \tag{42}$$

and $\aleph_{n\ell}$ is the normalization constant

RESULTS AND DISCUSSION

The obtained numerical results of this study are discussed in this section. To do all the following calculations, the parameters are taken as follows: $D_e = 2.05\ eV, r_e = 1.781$ Å, $\delta = 1.32408$ Å^{-1}, $\mu = 0.987371$ a. m. u, $\hbar c = 1973.269\ eV$Å and $1\ a.m.u = 931.494028\ MeVc^{-2}$ (Oyewumi *et al.*, 2014). The numerical results are presented in Tables 1, 2, and 3 for three different cases. Case 1: Slope parameter $\tilde{g} = -1$. For this case, both positive and negative energy values occur for all quantum states. A clear trend of decreasing energy with increasing n is observed across all configurations and magnetic quantum numbers. When both the magnetic and AB-flux fields are set to zero, the system exhibits degeneracy across $m = \pm 1$. When a magnetic field is applied while the AB-flux field remains zero, this degeneracy is lifted, and separate energy levels appear for each value of m. Both positive and negative energy levels shift downward. When the magnetic field is removed, but a non-zero AB-flux is present, quasi-degeneracy appears as a partial overlap in the energies of $m = \pm 1$. In this case, the energy values also decrease compared to the field-free case. When both magnetic and AB-flux fields are non-zero, the strongest degeneracy lifting occurs. This configuration results in the lowest positive energy values and the most negative energy values among the four cases, indicating that the combined fields have a stronger perturbative effect than either field alone. Case 2: Slope parameter $\tilde{g} = 0$. In this table, only positive energy values are obtained for all field configurations and quantum states. For each value of m, energy decreases with increasing n, maintaining a consistent trend. Compared to Table 1 ($\tilde{g} = -1$), the energy spectrum is shifted upward.

Table 1: Numerical Eigenvalues of the Modified Kratzer Energy-Dependent Screened Coulomb Potential (MKEDSCP) for TiH Diatomic Molecule with various $n$and mQuantum States for Energy Coefficient $\tilde{g} = -1$with the impact of magnetic $\vec{B}$ field and AB-flux field $\vec{\xi}$

$E_{nm}(eV)$		TiH	$\tilde{g} = -1$		
m	n	$E_{nm}(\tilde{B} = \tilde{\xi} = 0)$	$E_{nm}(\tilde{B} = 0.001, \tilde{\xi} = 0)$	$E_{nm}(\tilde{B} = 0, \tilde{\xi} = 0.001)$	$E_{nm}(\tilde{B} = \tilde{\xi} = 0.001)$
	0	0.5726200299, −15.27371997	2.432351424, −46.52985936	0.5726207212, −15.27373621	0.3756109053, −71.90812628
	1	0.5288093857, −15.78517790	2.344753331, −47.71546815	0.5288100836, −15.78519432	0.2585360109, −73.26172860
-1	2	0.4839029615, −16.30537954	2.255383526, −48.90914474	0.4839036650, −16.30539614	0.1402175036, −74.62392680
	3	0.4379112255, −16.83433535	2.164287178, −50.11093421	0.4379119352, −16.83435213	0.02066907465, −75.99473456
	0	0.5722747938, −15.26560772	2.507451526, −45.46303645	0.5722747938, −15.26560772	0.4639818710, −70.85516157
	1	0.5284604579, −15.77697320	2.421517363, −46.64144075	0.5284604579, −15.77697320	0.3478976206, −72.20209169
0	2	0.4835506997, −16.29708274	2.333766820, −47.82786820	0.4835506997, −16.29708274	0.2305582296, −73.55760615
	3	0.4375559780, −16.82594681	2.244248144, −49.02236698	0.4375559781, −16.82594682	0.1119779592, −74.92171921
	0	0.5726200299, −15.27371997	2.585500478, −44.41461486	0.5726193400, −15.27370375	0.5551377465, −69.82044022
	1	0.5288093857, −15.78517790	2.501218321, −45.58581740	0.5288086879, −15.78516150	0.4400254835, −71.16070582
1	2	0.4839029615, −16.30537954	2.415074437, −46.76499765	0.4839022563, −16.30536295	0.3236468771, −72.50954456
	3	0.4379112255, −16.83433535	2.327120257, −47.95220711	0.4379105147, −16.83431858	0.2060167532, −73.86697128

Table 2: Numerical Eigenvalues of the Modified Kratzer Energy-Dependent Screened Coulomb Potential (MKEDSCP) for TiH Diatomic Molecule with Various $n$and mQuantum States for Energy Coefficient $\tilde{g} = 0$with the Impact of Magnetic $\vec{B}$ Field and AB-flux Field $\vec{\xi}$

$E_{nm}(eV)$		TiH	$\tilde{g} = 0$		
m	n	$E_{nm}(\tilde{B} = \tilde{\xi} = 0)$	$E_{nm}(\tilde{B} = 0.001, \tilde{\xi} = 0)$	$E_{nm}(\tilde{B} = 0, \tilde{\xi} = 0.001)$	$E_{nm}(\tilde{B} = \tilde{\xi} = 0.001)$
	0	1.320653216	3.217928668	1.320655361	0.5749703663
	1	1.216561505	3.132291088	1.216563604	0.3978471323
-1	2	1.110582030	3.041271046	1.110584083	0.2168830982
	3	1.002716953	2.944975098	1.002718963	0.03213034432
	0	1.319581582	3.287034129	1.319581582	0.7072201400
	1	1.215512008	3.206366054	1.215512009	0.5331404637
0	2	1.109554387	3.120215362	1.109554388	0.3551779056
	3	1.001710905	3.028692387	1.001710904	0.1733859235
	0	1.320653216	3.358238763	1.320651074	0.8426097547
	1	1.216561505	3.282577986	1.216559406	0.6715662430
1	2	1.110582030	3.201332158	1.110579972	0.4965974162
	3	1.002716953	3.114615500	1.002714938	0.3177581317

Table 3: Numerical Eigenvalues of the Modified Kratzer Energy-Dependent Screened Coulomb Potential (MKEDSCP) for TiH Diatomic Molecule with Various $n$and mQuantum States for Energy Coefficient $\tilde{g} = 1$with the Impact of Magnetic $\vec{B}$ Field and AB-flux Field $\vec{\xi}$

$E_{nm}(eV)$		TiH	$\tilde{g} = 1$		
m	n	$E_{nm}(\tilde{B} = \tilde{\xi} = 0)$	$E_{nm}(\tilde{B} = 0.001, \tilde{\xi} = 0)$	$E_{nm}(\tilde{B} = 0, \tilde{\xi} = 0.001)$	$E_{nm}(\tilde{B} = \tilde{\xi} = 0.001)$
	0	3.773706846, −2.317625174	3.770716533, −30.01471170	3.773714435, −2.317625775	1.146192329, −23.56452380
	1	3.755946592, −2.222435816	3.752064496, −29.81851805	3.755954296, −2.222436502	0.8222438013, −23.03549754
-1	2	3.728502443, −2.116190499	3.725065040, −29.61260493	3.728510276, −2.116191285	0.4656187223, −22.47242266
	3	3.690195987, −1.997710812	3.689352746, −29.39660690	3.690203968, −1.997711721	0.07181908109, −21.87080115
	0	3.769913569, −2.317327002	3.776897561, −30.18253957	3.769913574, −2.317327000	1.372533159, −23.95243440
	1	3.752096223, −2.222092927	3.765425939, −29.99476299	3.752096228, −2.222092925	1.071298331, −23.44719037
0	2	3.724587607, −2.115795517	3.745912278, −29.79757229	3.724587611, −2.115795515	0.7402339659, −22.91074475
	3	3.686207301, −1.997254363	3.718013948, −29.59062489	3.686207305, −1.997254361	0.3755523907, −22.33930985
	0	3.773706846, −2.317625174	3.784326381, −30.34463637	3.773699263, −2.317624579	1.593241820, −24.32773315
	1	3.755946592, −2.222435816	3.779866720, −30.16510636	3.755938896, −2.222435128	1.313184189, −23.84473118
1	2	3.728502443, −2.116190499	3.767655600, −29.97645283	3.728494618, −2.116189704	1.005764069, −23.33299467
	3	3.690195987, −1.997710812	3.747371393, −29.77835417	3.690188014, −1.997709896	0.6677620971, −22.78930425

In the absence of both magnetic and AB-flux fields, degeneracy is present across $m = \pm 1$. When the magnetic field is applied alone, degeneracy is lifted and the highest energy values among all configurations are obtained, with the level spacing widening as the magnetic field strengthens. When the magnetic field is switched off but a non-zero AB-flux field is applied, quasi-degeneracy is observed at $m = \pm 1$, and the standard decrease of energy with increasing n persists. When both fields are non-zero, degeneracy is fully lifted and this combination yields the lowest energy values for this slope parameter. Case 3: Slope parameter $\tilde{g} = 1$. The same overall patterns observed for $\tilde{g} = -1$ are also present in this table. However, in this case, the positive energy values decrease, while for the negative energy, the energy values increase. This behavior reflects the influence of a positive slope parameter, which modifies the curvature of the effective potential and alters how sensitively the system responds to the external perturbations. Figure 1 presents the variation of the energy eigenvalues of the TiH diatomic molecule as a function of the external magnetic field B, in the absence of the Aharonov–Bohm (AB) flux field and for an energy slope parameter $\tilde{g} = 1$, corresponding to a magnetic quantum number $m = 1$. The curves represent the quantum states $n = 0,1,2,3$. A consistent trend is observed across all states. The energy eigenvalues increase sharply with increasing magnetic field strength in the low-B regime. Beyond a certain magnetic field threshold, the rate of increase diminishes and the curves exhibit saturation behavior, becoming asymptotic to an upper energy limit of approximately 3.8 eV. Among the quantum states, the ground state ($n = 0$) consistently attains the highest energy at each magnetic field value, followed in descending order by the excited states ($n = 1,2,3$). This ordering is preserved throughout the entire magnetic field range, with no level crossing observed for any magnetic quantum number considered.

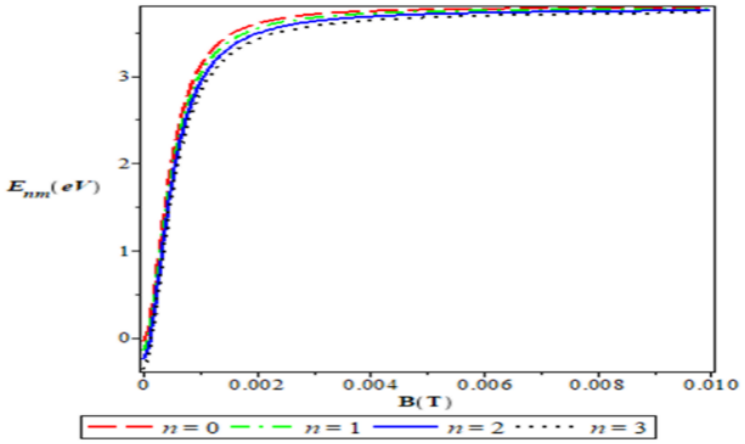

Figure 1: Variation of the Energy Eigenvalues of TiH Diatomic Molecule under the Influence of the Magnetic field for $m = 1$, $\tilde{g} = 1$and $\vec{\xi} = 0$

Figure 2 below illustrates the variation of the energy eigenvalues as a function of the external magnetic field B under the combined influence of a non-zero AB-flux field and an energy slope parameter $\tilde{g} = 1$, corresponding to $m = 1$. The curves again represent the quantum states $n = 0,1,2,3$. In this configuration, all energy eigenvalues exhibit a sharp decrease from their initial values at $B \approx 0$, reaching distinct minima around $B \approx 0.001$ T. The ground state ($n = 0$) attains the highest minimum energy, while the excited states ($n = 1,2,3$) display progressively lower minima, preserving their relative ordering. Beyond the minimum points, the energy eigenvalues increase gradually and smoothly with increasing magnetic field strength, accompanied by a growing separation between adjacent energy levels. At higher magnetic field values, the energy curves approach different saturation limits, approximately 1.2 eV, 1.4 eV, and 1.6 eV for the ground state, with corresponding but distinct saturation values for higher excited states, depending on the quantum state and magnetic quantum number.

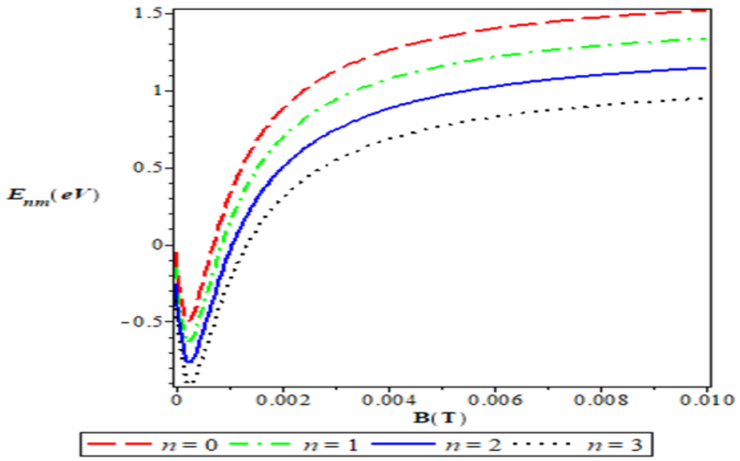

Figure 2: Variation of the Energy Eigenvalues of TiH Diatomic Molecule under the Influence of the Magnetic field for $m = 1$, $\tilde{g} = 1$and $\vec{\xi} = 0.001$

Figure 3 below depicts the variation of the energy eigenvalues with respect to the Aharonov–Bohm flux field in the absence of an external magnetic field, for an energy slope parameter $\tilde{g} = 1$ and magnetic quantum number $m = 1$. The quantum states $n = 0,1,2,3$ are shown as the coloured plots on the figure. In this case, the energy eigenvalues remain constant across the entire range of AB-flux values considered. The energy levels are clearly separated by a uniform positive spacing of approximately 0.1 eV between adjacent quantum states. The ground state $(n = 0)$ consistently exhibits the highest energy value (approximately 0.05 eV), while the excited states show monotonically decreasing energies with increasing n. The relative ordering of the energy levels remains unchanged for all magnetic quantum numbers.

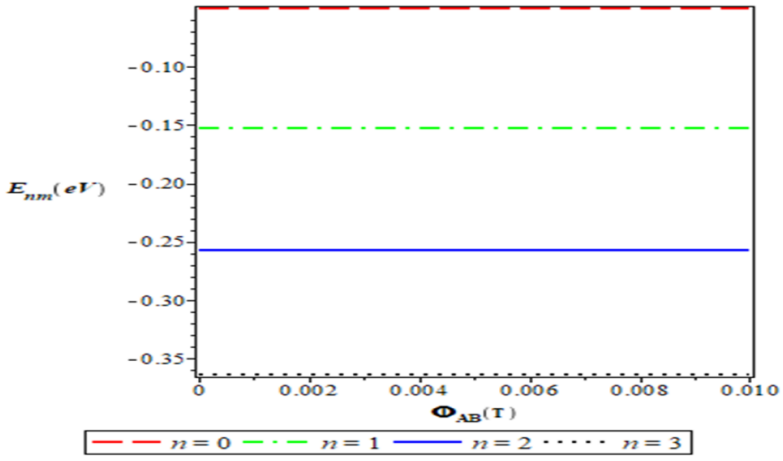

Figure 3: Variation of the Energy Eigenvalues of TiH Diatomic Molecule under the Influence of the AB-flux field for $m = 1$, $\tilde{g} = 1$and $\vec{B} = 0$

Figure 4 below shows the behavior of the energy eigenvalues as a function of the Aharonov–Bohm flux field in the presence of a non-zero magnetic field, with an energy slope parameter $\tilde{g} = 1$ and magnetic quantum number $m = 1$. For all quantum states, the energy eigenvalues decrease monotonically as the AB-flux field increases. The energy values initially start slightly above zero and rapidly transition into the negative energy domain as the AB-flux increases.

The spacing between adjacent energy levels becomes very small, giving rise to an almost degenerate spectrum, although the ground state $(n = 0)$ consistently remains the uppermost curve. The overall shape and ordering of the energy levels are preserved across the entire AB-flux range, with no level crossing or inversion observed.

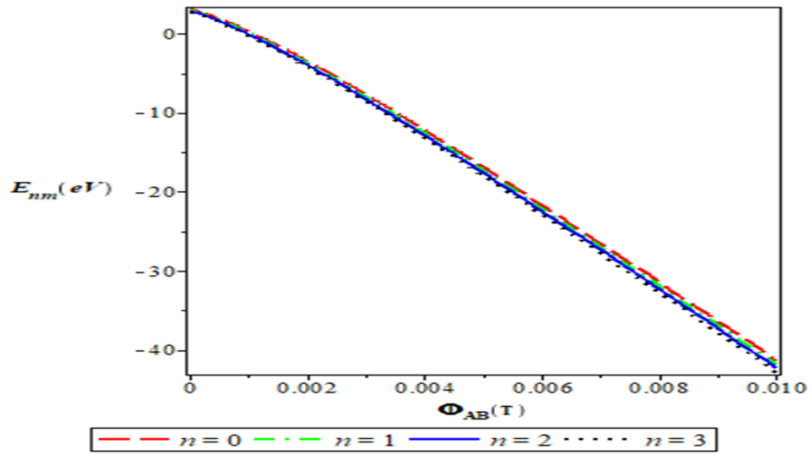

Figure 4: Variation of the Energy Eigenvalues of TiH Diatomic Molecule under the Influence of the AB-flux field for $m = 1$, $\tilde{g} = 1$and $\vec{B} = 0.001$

Since the result in Eq. (39) is new and there is no available literature with which to compare this study, we rather investigate the Special cases obtained by varying the magnetic quantum number and slope parameter reduce to the known modified Kratzer–Coulomb potential, and the resulting spectra agree well with available literature. By setting $m = \ell + \frac{1}{2}$ and $\tilde{g} = 0$ in Eq. (39), turns to be in the form:

$$E_{n\ell} = D_e - 2D_e\delta r_e + D_e\delta^2 r_e^2 + \frac{\hbar^2\delta^2\ell(\ell+1)}{2\mu} - \frac{\hbar^2\delta^2}{2\mu} \times \left[\frac{\frac{4\mu D_e r_e + 2\mu A}{\hbar^2\delta} - \frac{2\mu D_e r_e^2}{\hbar^2} - \ell(\ell+1) - \left(n+\frac{1}{2}+\sqrt{\frac{1}{4}+\frac{2\mu D_e r_e^2}{\hbar^2}+\ell(\ell+1)}\right)}{2\left(n+\frac{1}{2}+\sqrt{\frac{1}{4}+\frac{2\mu D_e r_e^2}{\hbar^2}+\ell(\ell+1)}\right)}\right]^2 \quad (43)$$

Equation (43) is consistent with the one obtained in Eq. (23) of (Edet *et al*., 2020). The numerical energy values of Eq. (43) are presented in tables 4 and 5 below:

Table 4: Comparison of the Numerical Eigenvalues (in eV) of Modified Kratzer Screened Coulomb Potential for Different Values of n and ℓ for Different Diatomic Molecules

n	ℓ	N_2 [NU] Edet et al., (2020)	N_2 [NUFA] (Present)	CO [NU] Edet et al., (2020)	CO [NUFA] (Present)
0	0	9.474983971	9.474994070	8.541820250	8.541831363
0		9.474953820	9.474964931	8.541790206	8.541711317
1	1	9.474959637	9.474959748	8.541796145	8.541796145
0		9.474923928	9.474934939	8.541760426	8.541771537
1	2	9.474929746	9.474939757	8.541766365	8.541777476
2		9.474941385	9.474952396	8.541778244	8.541789355
0		9.474894291	9.474895392	8.541730906	8.541741917
1		9.474900111	9.474911222	8.541736847	8.541747958
2	3	9.474911752	9.474922863	8.541748729	8.541759839
3		9.474929214	9.474939325	8.541766552	8.541777663
0		9.474864907	9.474875918	8.541701644	8.541712755
1		9.474870728	9.474881839	8.541707586	8.541718697
2	4	9.474882372	9.474893483	8.541719470	8.541729581
3		9.474899837	9.474899848	8.541737298	8.541738399
4		9.474923125	9.474934236	8.541761068	8.541762179
0		9.474835771	9.474846882	8.541672636	8.541783747
1		9.474841594	9.474852695	8.541678579	8.541789689
2		9.474853240	9.474864351	8.541690466	8.541791577
3	5	9.474870708	9.474871819	8.541708297	8.541819398
4		9.474894001	9.474885112	8.541732072	8.541843183
5		9.474923116	9.474934227	8.541761790	8.541872891

Table 5: Comparison of the Numerical Eigenvalues (in eV) of Modified Kratzer Screened Coulomb Potential for Different Values of n and ℓ for Different Diatomic Molecules

n	ℓ	NO [NU] Edet et al., (2020)	NO [NUFA] (Present)	CH [NU] Edet et al., (2020)	CH [NUFA] (Present)
0	0	6.303864689	6.303875790	3.124280611	3.124291722
0		6.303836703	6.303847814	3.124022422	3.124033533
1	1	6.303842142	6.303853253	3.124061521	3.124072632
0		6.303808986	6.303819107	3.123774225	3.123785336
1	2	6.303814426	6.303825537	3.123813539	3.123824640
2		6.303825311	6.303836422	3.123892189	3.123893299
0		6.303781534	6.303792645	3.123535425	3.123548536
1	3	6.303786975	6.303797906	3.123574942	3.123585953
2		6.303797863	6.303798974	3.123653997	3.123644998
3		6.303835965	6.303846976	3.123772630	3.123783741
0		6.303754342	6.303765453	3.123305474	3.123317586
1		6.303759786	6.303769897	3.123345183	3.123356294
2	4	6.303770676	6.303781787	3.123424620	3.123435731
3		6.303787009	6.303798110	3.123543823	3.123554934
4		6.303808788	6.303819899	3.123702849	3.123713951
0		6.303727408	6.303738519	3.123083866	3.123194977
1		6.303732853	6.303743964	3.123123755	3.123134866
2		6.303743746	6.303754857	3.123203553	3.123214664
3	5	6.303760084	6.303771195	3.123323296	3.123334397
4		6.303781868	6.303783980	3.123483035	3.123494146
5		6.303809097	6.303810018	3.123682842	3.123593953

CONCLUSION

This study has examined the influence of magnetic and Aharonov–Bohm flux fields on the Titanium Hydride (TiH) diatomic molecule using the modified Kratzer energy-dependent screened Coulomb potential. By applying the NUFA method, closed-form energy expressions were obtained and numerically evaluated for various values of the slope parameter $\tilde{g}$. The results reveal that the slope parameter plays a central role in shaping the molecular energy spectrum. Negative slope values ($\tilde{g} < 0$) allow both positive and negative bound-state energies, zero slope yields only positive states, while positive slope values ($\tilde{g} > 0$) influence the spacing and symmetry of the energy levels. External fields significantly modify degeneracy patterns in TiH. Magnetic fields remove degeneracy across $m = \pm 1$, AB-flux fields induce quasi-degeneracy, and the combined fields cause the strongest degeneracy lifting and the largest downward shift in energy. Across all cases, energy levels decrease with increasing vibrational quantum number n, and the special cases considered reduce smoothly to the known modified Kratzer–Coulomb solutions, confirming the accuracy of the model. Overall, the study demonstrates that both the slope parameter and external fields are powerful tools for tuning molecular energy spectra, with important implications for molecular control, spectroscopy and field-dependent molecular dynamics.

REFERENCES

Aygun, M., Bayrak, O., Boztosun, I., & Sahin, Y. (2012). The energy eigenvalues of the Kratzer potential in the presence of a magnetic field. *European Physical Journal D, 66*, 35, 1–5. https://doi.org/10.1140/epjd/e2011-20319-5

Cetin, A. (2008). A Quantum Pseudodot system with a two-dimensional Pseudoharmonic Potential, *Physics Letters A*, 372(21), 3852-3856.https://doi.org/10.1016/j.physleta.2008.02.037

Edet, C. O., Okorie, U. S., Ngiangian, A. T., & Ikot, A. N. (2020). Bound state solutions of the Schrödinger equation for the modified Kratzer potential plus screened Coulomb potential. *Indian Journal of Physics, 94*(4), 425–433. https://doi.org/10.1007/s12648-019-01477-9

Edet, C. O., Khordad, R., Ettah, E. B., Aljunid, S. A., Endut, R., Ali, N., Asjad, M., Ushie, P. O., & Ikot, A. N. (2022). Magneto-transport and thermal properties of TiH diatomic molecules under the influence of magnetic and Aharonov–Bohm (AB) fields. *Scientific Reports, 12*, 15430. https://doi.org/10.1038/s41598-022-19396-x

Eshghi, M., & Mehraban, H. (2017). Study of a 2D charged particle confined by magnetic and Aharonov–Bohm flux fields under the radial scalar power potential. *European Physical Journal Plus, 132*(3), 121. https://doi.org/10.1140/epjp/i2017-11379-x

Falaye, B. J., Ikhdair, S. M., & Hamzavi, M. (2015). Formula method for bound state problems. *Few-Body Systems, 56*(1), 63–78. https://doi.org/10.1007/s00601-014-0937-9

Ferkous, N., Boultif, A. & Sifour, M. (2019). On the Spin-1/2 Aharonov-Bohm Problem for Modified Poschl-Teller Potential, Physical Regularization and Self-Adjoint Extensions. *The European Physical Journal Plus,* 134, 258. https://doi.org/10.1140/epjp/i2019-12608-0

Ferkous, N. & Bounames, A. (2013). 2D Pauli Equation with Hulthen Potential in the Presence of Aharonov-Bohm Effect. *Communication Theoretical Physics*, 59(6), 679-683. https://ctp.itp.ac.cn/EN/Y2013/V59/106/679

Flügge, S. (1971). *Practical quantum mechanics II*. Springer.

Greene, R. L., & Aldrich, C. (1976). Variational wave functions for a screened Coulomb potential. *Physical Review A, 14*, 2363–2366. https://doi.org/10.1103/PhysRevA.14.2363

Horchani, R., Al-Aamri, H., Al-Kindi, N., Ikot, A. N., Okorie, U. S., Rampho, G. J. & Jelassi, H. (2021). Energy Spectra and Magnetic Properties of Diatomic Molecules in the Presence of Magnetic and AB Fields with the Inversely Quadratic Yukawa Potential. *European Physical Journal D,* 75:36, 1-13. https://doi.org/10.1140/epjd/s10053-021-00038-2

Ibekwe, E. E., Okorie, U. S., Emah, J. P., Iyang, E. P., & Ekong, S. A. (2021). Mass spectrum of heavy quarkonium for screened-Kratzer potential using series expansion method. *European Physical Journal Plus, 136*, 87. https://doi.org/10.1140/epjp/s13360-021-01090-y

Ikhdair, S. M., & Hamzavi, M. (2012). A quantum pseudodot system with two-dimensional pseudoharmonic oscillator in external magnetic and Aharonov–Bohm fields. *Physica B: Condensed Matter, 407*(21), 4198–4207. https://doi.org/10.1016/j.physb.2012.07.004

Ikhdair, S. M., Hamzavi, M., & Sever, R. (2012). Spectra of cylindrical quantum dots: The effect of electrical and magnetic fields together with AB flux field. *Physica B: Condensed Matter, 407*(23), 4523–4529. https://doi.org/10.1016/j.physb.2012.08.013

Ikot, A. N., Okorie, U. S., Amadi, P. O., Edet, C. O., Rampho, G. J., & Sever, R. (2020). Superstatistics of Schrödinger equation with pseudo-harmonic potential in external magnetic and Aharonov–Bohm fields. *Heliyon, 6*, e03738. https://doi.org/10.1016/j.heliyon.2020.e03738

Ikot, A. N., Okorie, U. S., Amadi, P. O., Edet, C. O., Rampho, G. J., & Sever, R. (2021). The Nikiforov–Uvarov functional analysis method: A new approach for solving exponential-type potentials. *Few-Body Systems, 62*, 9. https://doi.org/10.1007/s00601-021-01593-5

Jia, C. S., Zhang, L. H., & Wang, C. W. (2017). Thermodynamic properties for the lithium dimer. *Chemical Physics Letters, 667*, 211–215. https://doi.org/10.1016/j.cplett.2016.11.059

Karayer, H., Demirha, D., & Buyukkilic, F. (2015). Extension of Nikiforov–Uvarov method for the solution of Heun equation. *Journal of Mathematical Physics, 56*, 063504. https://doi.org/10.1063/1.4922601

Khordad, R. (2010). Simultaneous effects of temperature and pressure on the donor binding energy in a V-groove quantum wire. *Superlattices and Microstructures, 47*(3), 422–431.

Nikiforov, A. F., & Uvarov, V. B. (1988). *Special functions of mathematical physics*. Birkhäuser.

Onyenegecha, C. P., Njoku, I. J., Omame, A., Okereke, C. J. & Onyeocha, E. (2021). Dirac Equation and Thermodynamic Properties with Modified Kratzer Potential. *Heliyon, 7,* e08023, 1-8. https://doi.org/10.1016/j.heliyon.2021.e08023

Oyewumi, K. J., Falaye, B. J., Onate, C. A., Oluwadare, O. J., & Yahaya, W. A. (2014). Thermodynamic properties and approximate solutions of the Schrödinger equation with the shifted Deng–Fan potential model. *Molecular Physics, 112*, 127–141. https://doi.org/10.1080/00268976.2013.804960

Purohit, K. R., Parmar, R. H., & Rai, A. K. (2020). Bound state solution and thermodynamical properties of the screened cosine Kratzer potential under the influence of magnetic and Aharonov–Bohm flux fields. *Annals of*

Physics, 168335. https://doi.org/10.1016/j.aop.2020.168335

Rampho, G. J., Ikot, A. N., Edet, C. O., & Okorie, U. S. (2020). Energy spectra and thermal properties of diatomic molecules in the presence of magnetic and AB fields with improved Kratzer potential. *Molecular Physics*, e1821922. https://doi.org/10.1080/00268976.2020.1821922

Serrano, F. A., Gu, X. Y. & Dong, S. H. (2010). Qiang–Dong proper quantization rule and its applications to exactly solvable quantum systems. *Journal of mathematical physics*, 51(8), 082103. https://doi.org/10.1063/1.3466802

Sever, R., Tezcan, C., Yesiltas, Ö., & Bucurgat, M. (2008). Exact solution of effective mass Schrödinger equation for the Hulthén potential. International Journal of Theoretical Physics, 47(9), 2243–2248. https://doi.org/10.1007/s10773-008-9656-7

Tezcan, C., & Sever, R. (2009). A general approach for the exact solution of the Schrödinger equation. *International Journal of Theoretical Physics, 48*(2), 337–350. https://doi.org/10.1007/s10910-007-9233-y